



## Electro Fenton process catalyzed by Fe@Fe<sub>2</sub>O<sub>3</sub> nanowire for degradation of carbamazepine from aqueous solutions

Mohammad Mehdi Amin<sup>a,b</sup>, Saeed Yousefinejad<sup>c</sup>, Mansooreh Dehghani<sup>d</sup>,  
Somayeh Rahimi<sup>b,e,\*</sup>

<sup>a</sup>Environment Research Center, Research Institute for Primordial Prevention of Non-communicable disease, Isfahan University of Medical Sciences, Isfahan, Iran, email: amin@hlth.mui.ac.ir

<sup>b</sup>Department of Environmental Health Engineering, School of Health, Isfahan University of Medical Sciences, North Bahonar Street, 8 Alley, Shiraz, Iran, Tel. +00989178368651; email: rahimi.somaye@gmail.com

<sup>c</sup>Research Center for Health Sciences, Institute of Health, Department of Occupational Health Engineering, School of Health, Shiraz University of Medical Sciences, Shiraz, Iran, email: Yousefisa@sums.ac.ir

<sup>d</sup>Research Center for Health Sciences, Institute of Health, Department of Environmental Health, School of Health, Shiraz University of Medical Sciences, Shiraz, Iran, email: mdehghany@sums.ac.ir

<sup>e</sup>Student Research Committee, School of Health, Isfahan University of Medical Sciences, Isfahan, Iran

Received 22 September 2018; Accepted 20 April 2019

### ABSTRACT

In this study, Fe@Fe<sub>2</sub>O<sub>3</sub> nanowires were applied in combination with electro Fenton (EF) process to decompose of carbamazepine (CBZ) drug in an electrochemical reactor using a graphite rod cathode and Ti/PbO<sub>2</sub> anode. Response surface methodology (RSM) based on central composite design was used to optimize various parameters such as pH, current, FeSO<sub>4</sub>·7H<sub>2</sub>O, drug and Fe@Fe<sub>2</sub>O<sub>3</sub> concentrations, and reaction time. The results of RSM showed a good statistical relationship between experimental values of CBZ removal and their predicted values using the suggested multi-parameter model. The efficacy of CBZ removal significantly enhanced with increasing density, Fe@Fe<sub>2</sub>O<sub>3</sub> nanowire dose, and reaction time, while it was reduced with increasing pH, FeSO<sub>4</sub>·7H<sub>2</sub>O concentration, and initial concentration of the drug. The results on a percentage of contribution and the *F*-value (PC% = 42.99 and *F* = 346.4003) showed that Fe@Fe<sub>2</sub>O<sub>3</sub> dose plays an important role in increasing the efficiency of the electro Fenton process. RSM results also revealed that EF process effectively removed 88.55% of CBZ and 65% of total organic carbon from aqueous solutions under optimum conditions; that is pH = 4, current = 0.18 A (current density = 5.14 mA cm<sup>-2</sup>), FeSO<sub>4</sub>·7H<sub>2</sub>O concentration = 3.87 mg L<sup>-1</sup>, CBZ concentration = 7.49 mg L<sup>-1</sup>, Fe@Fe<sub>2</sub>O<sub>3</sub> dose = 1,050 mg L<sup>-1</sup>, and reaction time = 50 min. The utilized multi-parameter optimization approach revealed the presence of interactions between pH with FeSO<sub>4</sub>·7H<sub>2</sub>O concentration and pH with reaction time. As a conclusion EF process catalyzed by Fe@Fe<sub>2</sub>O<sub>3</sub> nanowire can be used for the removal of pharmaceutical compounds such as CBZ from aqueous solutions.

**Keywords:** Electro Fenton; Carbamazepine; Fe@Fe<sub>2</sub>O<sub>3</sub> nanowire; Ti/PbO<sub>2</sub> Anode; Response surface methodology

### 1. Introduction

Pharmaceutical compounds have attracted intensive concerns as emerging pollutants in aquatic environment

in recent years. Owing to ever-increasing consumption, improper disposal and their imperfect removal in wastewater treatment plants (WWTPs), pharmaceutical compounds have been found everywhere in natural waters. Although most pharmaceuticals exist in the aquatic environment at

\* Corresponding author.

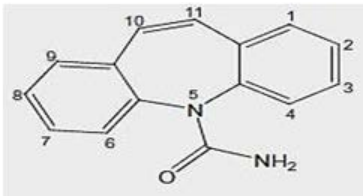
low level and indicates relatively low acute toxicity, it is possible that there are synergistic effects of pharmaceutical mixtures and continuous exposure to these compounds leads to negative impact on ecosystem [1]. In recent decades, the presence of pharmaceutical compounds in aquatic environments has been considered one of the critical environmental issues. Due to their polarity, low volatility, and high resistance to biological processes, many pharmaceutical compounds are not removed by the wastewater treatment processes; therefore, continuously enter receiving water bodies [2]. CBZ (Table 1), one of the dibenzazepine derivatives, is used for the treatment of bipolar disorder and trigeminal neuralgia [3,4]. This pharmaceutical combination has been identified frequently in aquatic environments due to its widespread use, high resistant properties and insufficient efficacy of effluent treatment (<10%) [5,6]. Most studies revealed that long-term exposure to this pharmaceutical resulted in reduced enzymatic activity, biological accumulation in various organisms, morphological changes, and limited growth of organisms in the environment [6,7]. Therefore, the removal of these pharmaceutical compounds from aqueous solutions is very prominent.

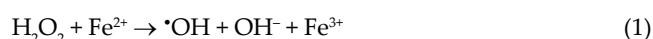
Various treatment methods such as adsorption [8], membrane separation [9], chemical oxidation [10] and photocatalytic degradation [11] have been used to remove CBZ from aqueous solutions. However, these physicochemical processes are not suitable for the removal of pharmaceutical compounds. For example, adsorption and membrane separation processes lead to transfer of pollutants from one phase to the other without being decomposed. Chemical oxidation has low efficiency in the mineralization of persistent organic pollutants [12]. The TiO<sub>2</sub> photocatalytic process has

some disadvantages such as low mineralization efficiency, a high cost of a light source, and requiring an additional separation step for the removal of TiO<sub>2</sub> catalyst during the process [12]. Advanced oxidation processes are needed to achieve complete decomposition of toxic and persistent pollutants to overcome these problems [12]. In recent years, advanced oxidation processes (AOPs) have become one of the most promising technologies for treating wastewater containing toxic and persistent pollutants [13].

These processes are based on the production of highly oxidizing species, such as hydroxyl radicals, which are capable of decomposing a wide range of non-degradable pollutants quickly without producing harmful products [6,13,14]. Due to its high efficiency, the simplicity of control, low cost and low toxicity of reagents, Fenton process, among AOPs, has been considered as a practical and attractive technology for degrading a large number of hazardous and persistent pollutants [6,15]. In this process, hydrogen peroxide (H<sub>2</sub>O<sub>2</sub>) is catalyzed by a ferrous ion to produce hydroxyl radicals (Eq. (1)) [16]. However, this technology has various disadvantages such as the rapid consumption of ferrous ions and the production of ferric sludge [17,18]. To overcome this problem, some researchers have demonstrated that EF oxidation offers significant benefits such as high efficiency for the removal of organic pollutants and needs no specific equipment [19,20]. This process has several other advantages, including continuous production of H<sub>2</sub>O<sub>2</sub> (Eq. (2)), low oxidation time and Fe<sup>2+</sup> reduction by direct reduction of Fe<sup>3+</sup> at the cathode (Eq. (3)) [17]. However, there are still some drawbacks, including isolation of residual ferric ions, efficiency in acidic pH, and the high cost of an iron anode in the EF process that should be addressed. To overcome these disadvantages, the researchers have proposed a solid catalyst containing iron species and development of titanium-based stable anodes [21–23].

Table 1  
Physical, chemical and pharmacological properties of carbamazepine

Carbamazepine (CBZ)	
Structure	
Formula	C <sub>15</sub> H <sub>12</sub> N <sub>2</sub> O
CAS No	298-46-4
Usage	Analgesic, antiepileptic
Molecular weight	236.27 g mol <sup>-1</sup>
Water solubility	17.7 mg L <sup>-1</sup> (25°C)
Log P (octanol–water)	2.45
Henry's law constant	1.09 × 10 <sup>-5</sup> Pa m <sup>3</sup> mol <sup>-1</sup> (25°C)
pKa	Neutral
Elimination half-life	25–65 h
Excretion	72% of oral dosage excreted in urine and 28% in faeces
Dosage	Maintenance usually 800–1,200 mg daily



In the EF process, the characteristics of the anode electrode are one of the main factors. Recently different types of anodes, including SnO<sub>2</sub>, PbO<sub>2</sub>, RuO<sub>2</sub>, IrO<sub>2</sub>, TiO<sub>2</sub>-RuO<sub>2</sub>-IrO<sub>2</sub>, Pt and boron-doped diamond (BDD) have been evaluated [24]. Among them, PbO<sub>2</sub> is a low-cost electrode material that is relatively stable at the high current flow and has a high potential for oxygen evolution [24,25]. During the oxidation of solutions containing pollutant, produced OH radicals on the surface of PbO<sub>2</sub> electrode directly decompose the pollutant without reacting with the surface of the anode. Different studies have highlighted the high mineralization of various types of pollutants by Ti/PbO<sub>2</sub> electrode [26]. For heterogeneous EF systems, the presence of limited working pH range, reusability of iron reagent and high oxidation efficiency at pH > 4 are very satisfactory. Hence, special attention has been paid to the development of iron reagents with high oxidation efficiency and recycling ability [27,28]. In recent years, Fe@Fe<sub>2</sub>O<sub>3</sub> core-shell nanowire has expanded as a nano zero-valent iron for decomposing

different pollutants. These nanowires lead to the production of reactive oxygen species (ROS) such as superoxide ( $\cdot\text{O}_2^-$ ) and hydrogen peroxide ( $\text{H}_2\text{O}_2$ ) through activating single and double electron molecular oxygen [29]. The production of these oxidants, through activation of molecular oxygen in Fenton processes, not only increases the number of ROS but also accelerates the reduction of ferric ions to ferrous ions. Hence, the replacement of  $\text{Fe@Fe}_2\text{O}_3$  with  $\text{Fe}^{2+}$  can contribute overcoming the common EF problems and results in high efficiency at  $\text{pH} > 4$  [30–32].

Given that no study has been done on the decomposition of CBZ by  $\text{Ti/PbO}_2$  anode and  $\text{Fe@Fe}_2\text{O}_3$  iron reagent. This study was attempted primarily to evaluate the efficacy of the EF process in the removal of CBZ and second to determine the optimum status by use of response surface methodology (RSM). Moreover, the effect of pH, current,  $\text{FeSO}_4 \cdot 7\text{H}_2\text{O}$  concentration, initial concentration of the drug, nanowire dose and electrolysis time on CBZ removal was investigated.

## 2. Materials and methods

### 2.1. Reagents and materials

Carbamazepine (CBZ, CAS No. 298-46-4,  $\text{C}_{15}\text{H}_{12}\text{N}_2\text{O}$ , and  $236.67 \text{ g mol}^{-1}$ ) was bought from Sigma-Aldrich (USA). Chemical co-precipitation method was utilized to prepare the  $\text{Fe@Fe}_2\text{O}_3$  nanowire using  $\text{FeCl}_3 \cdot 6\text{H}_2\text{O}$  as a precursor and  $\text{NaBH}_4$  as a reducing agent [33]. The acetonitrile and water (HPLC grade) were prepared from the Merck Company (Germany) and Sigma-Aldrich (USA), respectively. In this experiment, the grade reagents are applied devoid of being purified. Besides, working solutions were made ready by diluting CBZ at the needed range for every working day.

### 2.2. Preparation and characterization of $\text{Fe@Fe}_2\text{O}_3$ nanowire

In this study, a high-purity titanium plate (>99%) with a thickness of 1 mm was used to prepare the  $\text{Ti/PbO}_2$  anode electrode. Before preparation of the electrode, a titanium plate ( $5 \text{ cm} \times 7 \text{ cm}$ ) was mechanically polished by 320 grit paper strips to remove the  $\text{TiO}_2$  surface layer and increase the surface roughness. Then, the plate was immersed for 15–20 min in a concentrated solution of hydrochloric acid to remove organic residues on the surface. Next, the product was entirely washed with deionized water. To end with, the cleaned titanium plate was transferred to an electrochemical deposition cell containing 0.5 M of  $\text{Pb}(\text{NO}_3)_2$ , 0.05 M of NaF and 0.1 M of  $\text{HNO}_3$ . The electrodeposition process was performed by inserting Ti plate as anode and graphite bar as cathode. Moreover, the electrodeposition of  $\text{PbO}_2$  was performed at a constant current density of  $20 \text{ mA cm}^{-2}$  for 30 min with continuous mixing [34]. After the preparation of  $\text{Ti/PbO}_2$  electrode anode, the physical and structural properties of this electrode were determined through standard methods of scanning electron microscopy (Tescan SEM Mira 3, USA) and X-ray dispersion device (D8 Advance, Bruker, Germany).

### 2.3. Preparation of $\text{Ti/PbO}_2$ electrode

The  $\text{Fe@Fe}_2\text{O}_3$  nanowire was synthesized according to previous report [31]. The physical and structural properties

of these nanowires were determined using standard methods of scanning electron microscopy (Tescan SEM Mira 3, USA) and X-ray dispersion device (D8 Advance, Bruker, Germany) and energy dispersive X-ray analysis (EDX) were performed on a scanning electron microscope (SAMX).

### 2.4. Laboratory methods

CBZ decomposition tests were carried out in a 500 mL reactor at room temperature. The prepared  $\text{Ti/PbO}_2$  was applied as the anode and graphite bar as the cathode. The distance between the anode and the cathode was kept at 1 cm. In all tests, the solution was mixed with a magnetic stirrer. An air compressor provided the air needed to mix and the oxygen required for generating an  $\text{H}_2\text{O}_2$  cathode with a constant flow rate of  $1 \text{ L min}^{-1}$ .

The DC power supply (MEGATEK, MP-3003D, 3 A, 30 V) was used to regulate the electric current of the reactor. 0.1 M of sodium sulfate ( $\text{Na}_2\text{SO}_4$ ) was utilized as supporting electrolyte under different conditions of the designed variables. Electrochemical oxidation tests were performed by reacting different amounts of  $\text{Fe@Fe}_2\text{O}_3$  ( $0\text{--}1,400 \text{ mg L}^{-1}$ ) in 500 mL of CBZ solution ( $3\text{--}19 \text{ mg L}^{-1}$ ) at different pH values (2.5–8.5), different  $\text{FeSO}_4 \cdot 7\text{H}_2\text{O}$  ( $1\text{--}9 \text{ mg L}^{-1}$ ), different current (0.05–0.25 A (current densities  $1.43\text{--}7.14 \text{ mA cm}^{-2}$ )) and different electrolysis times (5–65 min). The initial pH of a synthetic solution of CBZ was adjusted via a pH meter and adding adequate amounts of NaOH (0.1 M) and HCl (0.1 M). Sampling from the reactor was done at different periods; the samples were filtered through a membrane filter with pore size  $0.22 \mu\text{m}$  and kept in the refrigerator (at most for 24 h) before analysis by high-performance liquid chromatography (HPLC).

### 2.5. Iron leaching test

The concentration of  $\text{Fe}^{2+}$  in solution will be measured with 1, 10-phenanthroline method and based on an amount of  $\text{Fe}^{2+}$  in used  $\text{Fe@Fe}_2\text{O}_3$  core-shell nanowire in optimum condition, and the amount of leached iron into solution had been calculated.

### 2.6. GC/MS analysis

The gas chromatography was performed with a fused silica capillary column ( $60 \text{ m} \times 0.25 \text{ mm i.d.}$ ,  $0.25 \mu\text{m}$  film thickness) to analyze the samples. The carrier gas was helium by a constant flow set at  $2 \text{ mL min}^{-1}$ . The temperature setting was at  $300^\circ\text{C}$  for the vaporization injector and the transfer line and  $230^\circ\text{C}$  for the ion source. The operation of the injector was assigned in 5:1 ratio split mode. The temperature of GC oven was set with a program, so that it started from  $120^\circ\text{C}$  held for 4 min, increased from  $120^\circ\text{C}$  to  $300^\circ\text{C}$  at  $20^\circ\text{C min}^{-1}$  rate, maintained at  $300^\circ\text{C}$  for 6 min, and finally with an absolute run time of 26 min. The analysis was done using scan mode.

### 2.7. Measurements and chromatographic analysis

HPLC instrument (Azura, Knauer, Berlin, Germany) equipped with a C18 column was utilized to identify the

concentration of CBZ. The applied HPLC was run by a diode array UV detector at a wavelength of 270 nm in isocratic elution mode. The used mobile phase was the mixture of acetonitrile/water (35:65 v/v) at a flow rate of 1 mL min<sup>-1</sup>. PTFE filter was used to filter the treated samples, and then the samples were injected into the 20 µL injection loop. Some samples detected by HPLC instrument did not require to be extracted, but samples with concentrations lower than the instrument's detection limit were extracted and then were injected into the HPLC instrument. In our work, dispersive liquid-liquid microextraction (DLLME) technique was applied as the extraction technique. In this approach, 1.0 mL of methanol as the dispersing solvent and 100 µL of chloroform as the extraction solvent were added into the sample. Adding these solvents caused the formation of a cloudy solution, which was centrifuged for 5 min at 5,000 rpm. Then, 30 µL of dropped sediment from DLLME extraction was taken with HPLC syringe and was injected into the device to ensure filling the injection loop. It is noteworthy that two calibration curves were prepared for lower concentration range after applying DLLME procedure and for higher concentration level without application of DLLME. Quantification of total organic carbon (TOC) was done via a Shimadzu TOC-VCPH analyzer (Japan) once desired samples filtered through a 0.22 µm filter.

Eq. (4) was applied to calculate the degradation efficiency of CBZ and TOC:

$$R(\%) = \frac{C_0 - C_e}{C_0} \times 100 \quad (4)$$

where  $C_0$  and  $C_e$  refer to the target compounds concentrations before and after the treatment in a reactor, respectively. The pH was measured through a Metrohm pH-meter 827 (Switzerland) equipped with a pH combined electrode.

### 2.8. Optimization and modeling of the response level

RSM is a well-known set of mathematical methods that have been applied to optimize many oxidation and removal processes. The number reduction of runs required to assess multiple parameters and their interactions can be noted as the main advantage of RSM. In the present study, the design of the runs and their statistical analysis were done based on RSM via Design-Expert software (version 7.0., Stat-Ease Inc., Minneapolis, USA). Central Composite Design (CCD) as an

RSM approach was used to optimize the variables of the EF process such as CBZ concentration, initial pH, reaction time, nanowires dose, FeSO<sub>4</sub>·7H<sub>2</sub>O concentration and current for CBZ treatment. Further, in the study, full factorial CCD suggested 81 samples of experiments concerning six factors in five levels in a single block. Five of these experiments were designed in the center levels of all factors, which are known as center points.

Six experimental factors of suggested reactor at five levels (-2, -1, 0, +1, +2) were taken into account as follows: pH (A), current (A) or current density (mA cm<sup>-2</sup>) (B), FeSO<sub>4</sub>·7H<sub>2</sub>O concentration (mg L<sup>-1</sup>) (C), CBZ concentration (mg L<sup>-1</sup>) (D), nanowires dose (mg L<sup>-1</sup>) (E), and reaction time (min) (F). Table 2 represents the operating ranges and levels of the applied independent variables of design.

A personal computer under Windows 7 operating system was applied to run Design-Expert software. Multiple linear regression (MLR) quadratic equation was the best case to clarify the interaction between the dependent and independent variables. For example, a quadratic model for  $x_1$  and  $x_2$  (as two independent variables) can be shown as follows (Eq. (5)):

$$Y = \beta_0 + \beta_1 x_1 + \beta_2 x_2 + \beta_{12} x_1 x_2 + \beta_{11} x_1^2 + \beta_{22} x_2^2 + \varepsilon \quad (5)$$

The variables in this equation are as follows:  $Y$  = efficiency of CBZ removal (dependent variable);  $\beta_0$  = intercept of MLR equation;  $\beta_1$  = coefficient of factor  $x_1$ ;  $\beta_{11}$  = self-interaction coefficients of factor  $x_1$ ;  $\beta_{22}$  = self-interaction coefficients of factor  $x_2$ ;  $\beta_{12}$  = interaction coefficient of the factors  $x_1$  and  $x_2$ .

As noted previously, six independent factors were applied to optimize the removal of CBZ in present work. The fitting performance in our model was expressed by the squared correlation coefficient ( $R^2$ ) and adjustment correlation coefficient ( $R^2_{adj}$ ).

## 3. Results and discussion

### 3.1. Fe@Fe<sub>2</sub>O<sub>3</sub> features

SEM and XRD investigated the morphology and Fe@Fe<sub>2</sub>O<sub>3</sub> nanowire compositions. Fe@Fe<sub>2</sub>O<sub>3</sub> morphology was in the form of the nanowire in the range of 40–80 nm and chain clusters formed through chemical reactions (Fig. 1). EDX showed that carbon, iron and oxygen were present in the sample (Fig. 2). The presence of iron and

Table 2  
Range of variables for the central composite design used to study the removal of CBZ during the suggested EF process

Independent variable	Code name	Star low (-α) (-2)	Low (-1)	Center (0)	High (+1)	Star high (+α) (2)
pH	A	2.5	4	5.5	7	8.5
Current (A) <sup>a</sup>	B	0.05	0.1	0.15	0.2	0.25
FeSO <sub>4</sub> ·7H <sub>2</sub> O concentration (mg L <sup>-1</sup> )	C	1	3	5	7	9
CBZ concentration (mg L <sup>-1</sup> )	D	3	7	11	15	19
Nanowires dose (mg L <sup>-1</sup> )	E	0	350	700	1,050	1,400
Oxidation time (min)	F	5	20	35	50	65

<sup>a</sup>Equal current density based on utilized electro surface (mA cm<sup>-2</sup>) = (1.43, 2.86, 4.29, 5.71, 7.14).

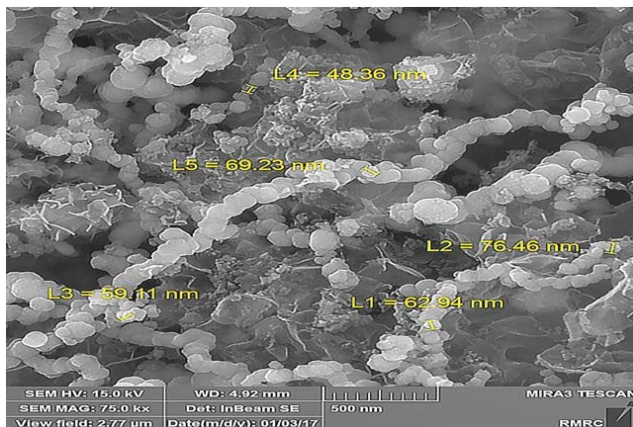


Fig. 1. SEM images of the synthesized Fe@Fe<sub>2</sub>O<sub>3</sub> nanowires.

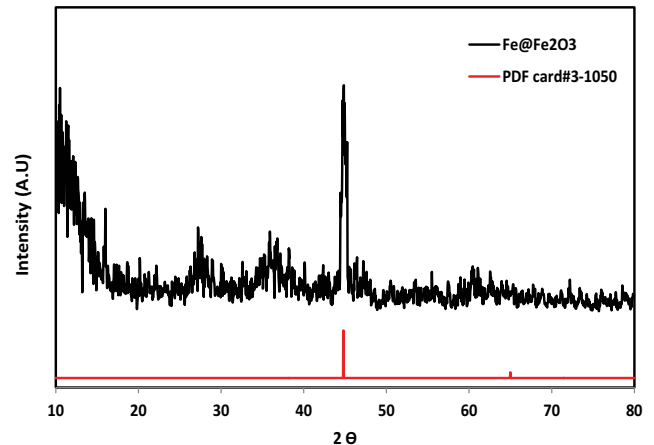


Fig. 3. XRD patterns of the synthesized Fe@Fe<sub>2</sub>O<sub>3</sub> nanowires.

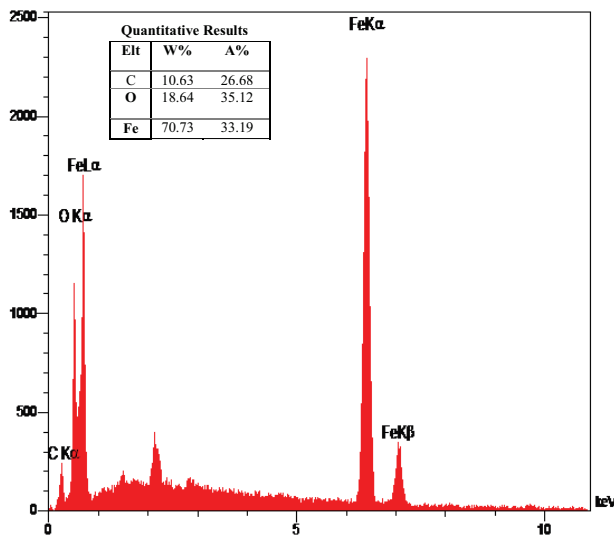


Fig. 2. Prepared EDX Fe@Fe<sub>2</sub>O<sub>3</sub>.

oxygen in the sample confirmed the nanowires' formation; whereas, carbon existed in the analyzed sample was entered from atmospheric carbon atoms [35]. The XRD analysis on nanowire revealed that the phase of the model occurred more in  $2\theta = 44.7^\circ$ , indicating the presence of cubic Fe (Fig. 3). These results are in line with previous studies [31,36,37].

### 3.2. Characteristics of the Ti/PbO<sub>2</sub> electrode

Figs. 4a and b display SEM and EDX micrograph of Ti/PbO<sub>2</sub> anode electrode synthesized by the electrodeposition process. As specified in Fig. 4a, a dense layer of lead dioxide was coated on the titanium plate. Energy dispersive X-ray spectroscopy (EDS) analysis confirmed the presence of lead and oxygen atoms on the Ti/PbO<sub>2</sub> electrode surface. The XRD pattern in Fig. 5 shows dispersion peaks at  $2\theta = 25.4^\circ, 32^\circ, 36.3^\circ, 49.2^\circ, 55.85^\circ, 59^\circ$  and  $62.5^\circ$ , which may be associated with specific peaks of tetragonal  $\beta$ -PbO<sub>2</sub> phase [38].

### 3.3. Synthesized Fe@Fe<sub>2</sub>O<sub>3</sub> nanowires for oxidation of CBZ

As highlighted in the methodology section, various parameters (pH, current, FeSO<sub>4</sub>·7H<sub>2</sub>O concentration, drug concentration, Fe@Fe<sub>2</sub>O<sub>3</sub> concentration and reaction time) were changed in five levels in order to optimize the conditions for the removal of CBZ (Table 2) and eventually 81 runs were designed. The values for each factor applied in the 81 runs are presented in Table S1. MLR and analysis of variance (ANOVA) were done to achieve the linear model related to the data presented in Table S1.

### 3.4. ANOVA and linear model of experimental design

Different multi-parameter models such as linear relationship, 2-factor interaction (2FI) and quadratic were evaluated to choose the best model, and results showed that quadratic model could be the best (Eq. (6)).

$$Y = b_0 + b_1A + b_2B + b_3C + b_4D + b_5E + b_6F + b_{12}AB + b_{13}AC + b_{14}AD + b_{15}AE + b_{16}AF + b_{11}A^2 + b_{22}B^2 + b_{33}C^2 + b_{44}D^2 + b_{55}E^2 + b_{66}F^2 \quad (6)$$

Due to enough number of experimental runs (81 runs), quadratic model use seems logical for suggested EF method. However, it should be noted that a model with a large number of parameters can cause overfitting. Hence, in such a case, good results can be obtained during the construction of a regression model, but poor ones may be achieved in the prediction step. For this reason, backward elimination was applied as the variable selection, and the variables (original variables or interactions) with *P*-values greater than 0.1 were removed. The final model suggested by CCD and after the variable selection is shown below:

$$\% \text{Efficiency} = 48.11 - 4.56A + 2.74B - 1.09C - 1.80D + 8.95E + 6.34F + 1.19AC + 0.88AF + 7.91A^2 \quad (7)$$

Based upon this equation, the positive coefficient sign of one factor denoted that the removal efficiency in suggested EF is increased when the factor level rises. On the other hand, the negative sign of one factor shows that as the factor level enhances, the removal efficiency of CBZ decreases.



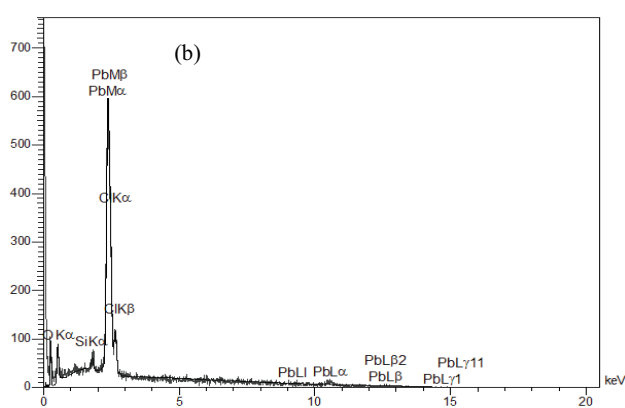


Fig. 4. (a) SEM micrograph of Ti/PbO<sub>2</sub> anode prepared by electrodeposition method and (b) EDS micrograph of Ti/PbO<sub>2</sub> anode prepared by electrodeposition method.

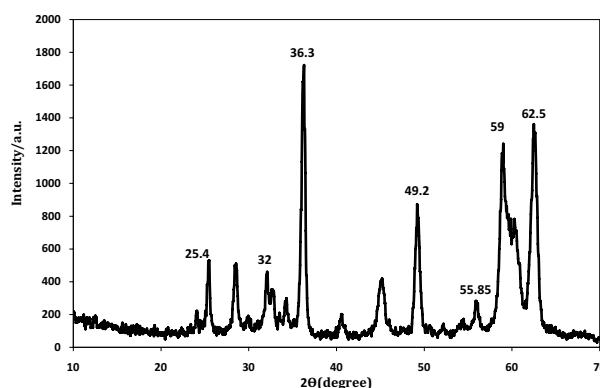


Fig. 5. X-ray dispersion pattern of Ti/PbO<sub>2</sub> anode prepared by electrodeposition.

ANOVA was done to assess the adequacy and significance of the EF models. *F*-value, *P*-value, *R*<sup>2</sup> (determination coefficient) and adjusted *R*<sup>2</sup> were used to indicate the accuracy and significance degree in the final regression models, which is represented in Table 3.

Moreover, validation of the final EF models was evaluated by the prediction correlation coefficient (*R*<sub>pred</sub><sup>2</sup>). As shown in Table 3, the *R*<sub>pred</sub><sup>2</sup> obtained was equal to 0.878, which confirms good predictability of the suggested model. Furthermore, the lack of fitness tests for this multi-parameter model was insignificant, confirming a proper fit and no significant residual.

On the other side, the high *F*-value in Table 3 indicates the most important factor in the CBZ removal efficiency that can be explained by the regression equation. *P*-value is used

Table 3  
ANOVA results on the multi-parameter model for CBZ oxidation by the EF process

Source	Sum of squares	df	Mean square	<i>F</i> -value	<i>P</i> -value prob > <i>F</i>	PC (%)
Model	13,186.7	9	1,465.189	87.84259*	<0.0001	
<i>A</i> -pH	1,501.219	1	1,501.219	90.00269	<0.0001	11.17
<i>B</i> -current (A)	541.6712	1	541.6712	32.47486	<0.0001	4.03
<i>C</i> -FeSO <sub>4</sub> ·7H <sub>2</sub> O concentration (mg L <sup>-1</sup> )	86.28382	1	86.28382	5.172981	0.0260	0.64
<i>D</i> -CBZ concentration (mg L <sup>-1</sup> )	235.0871	1	235.0871	14.0942	0.0004	1.75
<i>E</i> -nanoparticle dose	5,777.856	1	5,777.856	346.4003	<0.0001	42.99
<i>F</i> -reaction time (min)	2896.81	1	2896.81	173.6727	<0.0001	21.55
<i>AC</i>	91.91297	1	91.91297	5.510466	0.0217	0.68
<i>AF</i>	50.25215	1	50.25215	3.012772	0.0869	0.37
<i>A</i> <sup>2</sup>	2,005.607	1	2,005.607	120.2423	<0.0001	14.92
Residual	1,184.259	71	16.67971			
Lack of fit	1,166.56	67	17.41135	3.935016**	0.0938	
Pure error	17.69888	4	4.424721			
Cor total	14,370.96	80				
<i>R</i> <sup>2</sup>	0.918					
<i>R</i> <sub>adj</sub> <sup>2</sup>	0.9078					
<i>R</i> <sub>pred</sub> <sup>2</sup>	0.878					

\*Significant.

\*\*Not significant.

to estimate that  $F$  is large enough to represent the statistical significance of suggested EF model.

$P$ -value  $< 0.1$  specifies that the model conditions are significant at confidence level  $\geq 90\%$ . The results concerning  $F$ -value (87.84) and  $\text{prob} > F$  (0.0001) indicated that the model is statistically significant. The small amount due to lack of fit ( $P$ -value  $< 0.1$ ) showed that the quadratic model was suitable for the response. Table 3 also shows that catalyst amount ( $\text{PC}\% = 42.99$  and  $F = 346.4003$ ) was the most influential factor and  $\text{FeSO}_4 \cdot 7\text{H}_2\text{O}$  concentration ( $\text{PC}\% = 0.64$  and  $F = 5.17$ ) was the least influential one among the main factors. The effects of interaction terms were generally lower than that of main factors, and AC and AF interaction had the most significant effect on CBZ removal using the EF process. Among the second-order interactions, only the interaction between pH and pH ( $A^2$ ) was effective on the process due to high  $F$ -value and  $P$ -value  $< 0.1$ . The adequacy of the model was evaluated by plotting the distribution of residuals. The residual distribution around a straight line

in Fig. 6a shows its normal distribution in our constructed model. According to Fig. 6b, almost half the residuals were above, and the other half was below the zero lines, specifying that all the residues are distributed around zero, which indicates the exclusion of systematic error. On the other hand, Fig. 6b also indicates that the studentized (standardized) residuals of almost all 81 runs were in the acceptable range of  $\pm 3\sigma$  [39]. Fig. 6c demonstrates the actual and predicted oxidation efficiency rate of CBZ. As depicted in Fig. 6c, there is an acceptable correlation between the predicted oxidation rate of CBZ by the suggested model and their actual amounts. The amounts of correlation coefficients of the model ( $R^2 = 0.918$  and  $R^2_{\text{adj}} = 0.907$ ) and the correlation coefficients of prediction ( $R^2_{\text{pred}} = 0.878$ ) confirm the fitting potential and prediction ability of Eq. (7), respectively. Referring to these results, it may be concluded that the obtained model is sufficient to explain the relationship between the oxidation efficiency and operator factors for decomposition of CBZ through EF process.

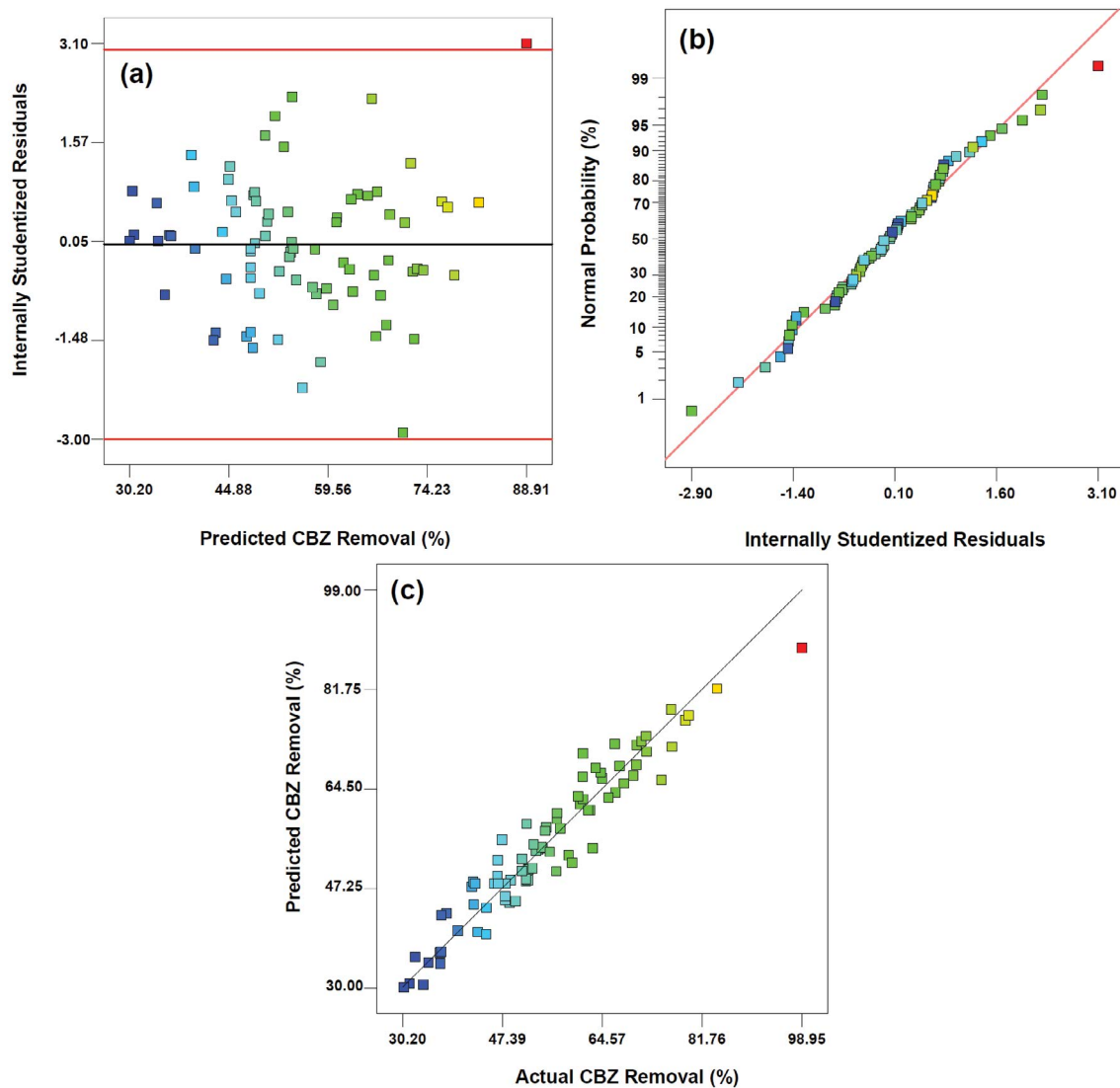


Fig. 6. Residual plots of EF system for CBZ removal: (a) normal probability plot of residuals, (b) range of studentized residual vs. predicted removal efficiency and (c) estimated value vs. laboratory values for decomposition efficiency.

### 3.5. Monitoring main effects

The effect of all single factors in our EF process (Fig. 7) and interactions between them (Fig. 8) were considered. The lines in these figures show the estimated changes in responses (CBZ removal efficiency) as each of the factors is altered from its lowest to highest levels.

### 3.6. Single factors

Graphical representations of variables linear effect were developed, and results are shown in Fig. 7. In this investigation, the effect of each factor was determined at pH of 5.5, the current of 0.15 A (current density = 4.28 mA cm<sup>-2</sup>), FeSO<sub>4</sub>·7H<sub>2</sub>O concentration of 5 mg L<sup>-1</sup>, CBZ concentration of 11 mg L<sup>-1</sup>, Fe@Fe<sub>2</sub>O<sub>3</sub> concentration of 700 mg L<sup>-1</sup>, and reaction time of 35 min.

### 3.7. Initial pH effect

As regarding drug oxidation, the effect of pH on catalyst species and the production/decomposition of H<sub>2</sub>O<sub>2</sub> is an important factor [40]. Clearly evident in Fig. 7a, the efficiency of drug removal reaches maximum using the EF

process at pH = 4. This reduction in the CBZ decomposition by increasing pH can be attributed to the restriction of the Fenton mechanism due to the reduction of H<sub>2</sub>O<sub>2</sub> concentration and the iron concentration in the solution. Furthermore, reduction of the radical amount of catalyzed hydroxyl by Fe@Fe<sub>2</sub>O<sub>3</sub> nanowires on the surface of the catalyst as well as spontaneous decomposition of H<sub>2</sub>O<sub>2</sub> may be a reason to reduce the drug removal rate at high pH [41]. At low pH, the formation of stable iron species with H<sub>2</sub>O<sub>2</sub> leads to catalyst deactivation and hydrogen peroxide stabilization by forming oxonium ion (Eq. (8)). At pH > 4, due to the instability of H<sub>2</sub>O<sub>2</sub>, this oxidant is rapidly decomposed into H<sub>2</sub>O according to Eq. (9) [42]. Previous studies have also shown that due to the availability of Fe<sup>2+</sup> and Fe<sup>3+</sup> on the catalyst surface, acidity status is appropriate to decompose pollutants via EF process [40].



In a study by Jiang et al. [41] on the decomposition of methyl orange color using a catalyzed EF process with

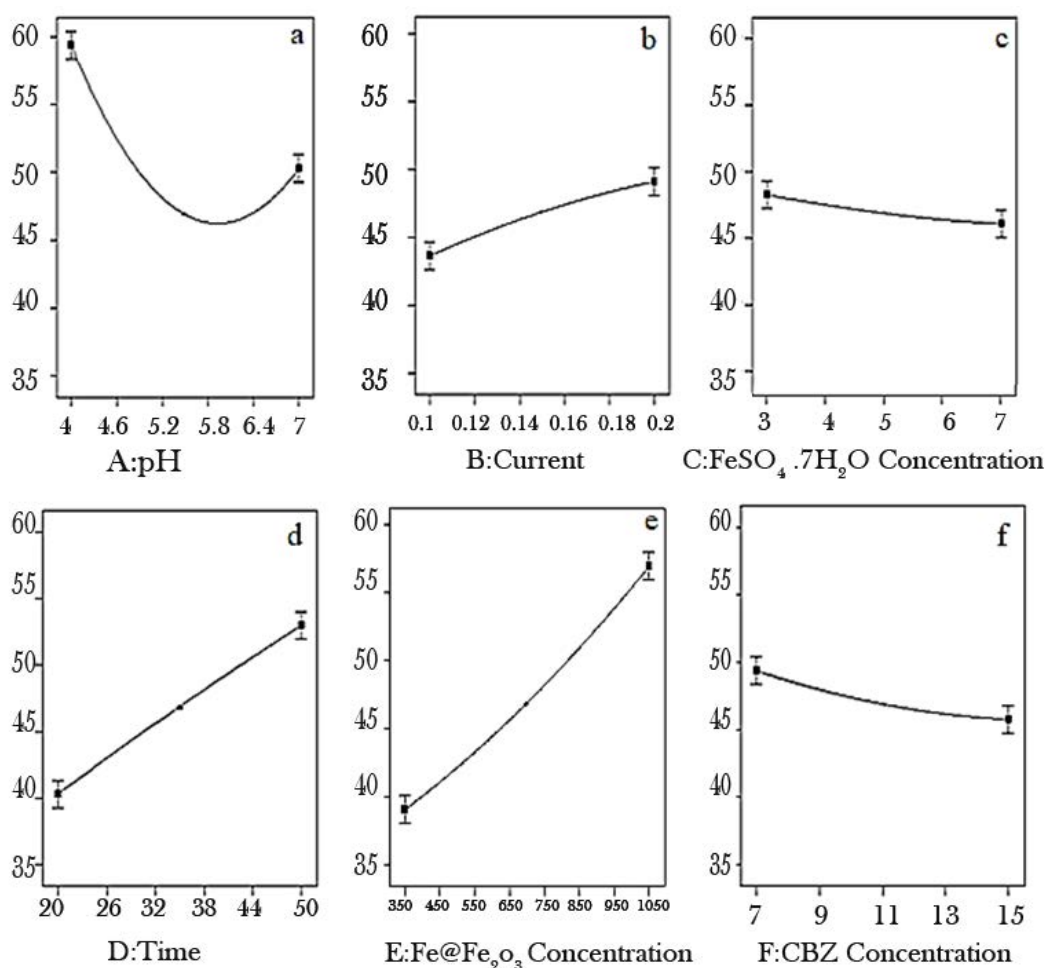


Fig. 7. Effect of various factors on CBZ removal via EF process: (a) effect of initial pH, (b) effect of current, (c) effect of FeSO<sub>4</sub>·7H<sub>2</sub>O initial concentration, (d) effect of reaction time, (e) effect of Fe@Fe<sub>2</sub>O<sub>3</sub> dose, and (f) effect of initial concentrations of CBZ.



magnetic Fe<sub>3</sub>O<sub>4</sub> nanoparticles, it was concluded that with the increase of initial pH, the color decomposition efficiency decreases. In a study by He et al. [42], the effect of initial pH was discussed using magnetic Fe<sub>3</sub>O<sub>4</sub> nanoparticles on the decomposition of reactive blue 19 color. The results revealed that the highest decomposition efficiency occurred at pH = 3, and due to H<sub>2</sub>O<sub>2</sub> instability, the color removal efficiency decreases with the increase of pH. Ai et al. [43] conducted a study on rhodamine B decomposition using EF process and Fe@Fe<sub>2</sub>O<sub>3</sub>/CNTs cathode. They reported that Fe@Fe<sub>2</sub>O<sub>3</sub>/CNTs cathode changes in different pH values. They suggested that in 120 min of reaction, decomposition rate reaches 99.6% in pH = 3 and 79.9% in pH = 8. Zhao et al. [44] concluded, after the oxidation of the pesticides EF, using Fe<sub>3</sub>O<sub>4</sub>@Fe<sub>2</sub>O<sub>3</sub>/activated carbon cathode, that by decreasing the pH from 6 to 3, the pesticides decomposition efficiency increases due to the production of high amounts of radical hydroxyl.

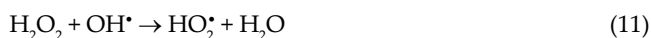
### 3.8. Effect of current

The current density is one of the most important operational parameters on the efficiency of the EF process due to the oxygen reduction and the hydrogen peroxide production at the cathode surface. Fig. 7b depicts the current effect on the oxidation of CBZ at a range of 0.1–0.2 A (current density 2.86–5.71 mA cm<sup>-2</sup>). As specified in this figure; the CBZ removal efficiency enhances when current increases. This increase in the oxidation rate can be attributed to the production of more H<sub>2</sub>O<sub>2</sub> by Eq. (2), resulting in the production of more hydroxyl radical from Fenton reaction (Eq. (1)) [45]. In addition, the electric production of Fe<sup>2+</sup> from Fe<sup>3+</sup> increases when current rises [46]. Also, the more CBZ molecules are adsorbed by increasing the current towards the electrode, thereby increasing the collision between the radical hydroxyl and the CBZ molecules. Additionally, at a proper current, particles are polarized in the form of microelectrodes that may increase the oxidation and electro-absorption process. Similar upshots were obtained by Panizza and Cerisola [45] for color decomposition in aqueous solutions. In their research, it has been reported that with increasing current density, the color decomposition rate is increased by the production of radical hydroxyl (Eq. (1)) and hydrogen peroxide (Eq. (2)). Yu et al. [47] concluded that, by the effect of current density on H<sub>2</sub>O<sub>2</sub> electric production, the production rate of H<sub>2</sub>O<sub>2</sub> was increased. Yahya et al. [48] analyzed the moxifloxacin antibiotic decomposition through the EF process and found that by increasing the current density efficiency, the antibiotic removal would be increased due to the production of high H<sub>2</sub>O<sub>2</sub> and Fe<sup>2+</sup> reduction. Pourzamani et al. [49] assessed three dimensional MWCNTs/Fe<sub>3</sub>O<sub>4</sub> based EF process and concluded that increasing flow density from 10 to 20 mA cm<sup>-2</sup> enhances the yield of diclofenac decomposition by producing high amounts of hydroxyl radical due to faster production of H<sub>2</sub>O<sub>2</sub> and faster reduction of ferrous ions in cathode during enhancement of flow density. Also, Sruthi et al. [50] reported that increasing flow from 3 to 4 V improves the yield of COD removal by zeolite/iron oxide-magnesium catalyzed EF process. García-Gómez et al. [51] studied EF process for CBZ removal using Ti/PbO<sub>2</sub>

and Ti/BDD electrodes. They reported that flow density is one of the most important parameters which affects CBZ removal and the yield of CBZ removal improves by increasing flow density from 1 to 2 A.

### 3.9. Effect of FeSO<sub>4</sub>·7H<sub>2</sub>O initial concentration

The results considering the effect of FeSO<sub>4</sub>·7H<sub>2</sub>O initial concentration on the rate of CBZ removal indicated that the drug removal rate was reduced by increasing FeSO<sub>4</sub>·7H<sub>2</sub>O concentration (Fig. 7c). This reduction in the removal rate can be due to consumption of radical hydroxyl and produced H<sub>2</sub>O<sub>2</sub> by a high amount of iron ion according to Eqs. (10) and (11). In Eq. (11) HO<sub>2</sub> is an oxidant, but it has lower oxidation potential than radical OH [52]. Besides, active sites on the cathode top surface are likely to be occupied by iron ions, leading to a reduction in the number of effective sites on the cathode surface for producing H<sub>2</sub>O<sub>2</sub> [46]. Gökkuş and Yıldız [53] investigated the application of the EF process in medical WWTPs, and it was found that by further increasing the concentration of ferrous ions, the TOC removal efficiency is reduced by produced oxidants' use. By studying the effect of iron concentration on the imidazolium EF treatment, Bocos et al. [54] reported that by increasing the concentration of Fe<sup>2+</sup>, the contaminant decomposition efficiency decreases due to the use of radical hydroxyl by extra Fe<sup>2+</sup>. Moreover, parallel results were reported by Zhang et al. [55] for the decomposition of 2,4-dichlorophenol by containing the EF system coupled with iron-containing carbon, also Iglesias et al. [56] results were reported for the oxidation of imidacloprid by a catalyzed EF process by iron-containing alginates gel. Wang et al. [57] reported that presence of Fe<sup>2+</sup> significantly enhances the yield of COD removal. COD removal percentage significantly increases by adding 0.33 mmol L<sup>-1</sup> external iron concentration from 19.8% to 43.1%. Zhou et al. [58] reported that presence of Fe<sup>2+</sup> increases the yield of methyl red removal from 45% to 75% in 10 min.



### 3.10. Effect of reaction time

According to Fig. 7d, the rate of CBZ decomposition increases when contact time rises from 20 to 50 min. The increase of drug decomposition by an increase of reaction time can be attributed to the formation of more radical hydroxyl on Ti/PbO<sub>2</sub> anode surface and the reaction between Fe<sup>2+</sup> and H<sub>2</sub>O<sub>2</sub> catalysts. Iranpour et al. [59] investigated the removal optimization of reactive black color 5 by the MWCNTs/Fe<sub>3</sub>O<sub>4</sub> based EF process, and reported that by increasing reaction time, the color decomposition efficiency is increased due to more contaminating contact with active catalyst sites, also production of high amounts of radical hydroxyl is increased by the reaction between Fe and H<sub>2</sub>O<sub>2</sub>. Mohammadi et al. [60] reported similar results about the removal of ibuprofen and naproxen drugs through the catalyzed EF process by iron-contained nickel foam.

### 3.11. Effect of Fe@Fe<sub>2</sub>O<sub>3</sub> dose

The amount of Fe@Fe<sub>2</sub>O<sub>3</sub> nanowire in solution is one of the important parameters in the EF process due to its key role in the reaction of Fenton and paving the way for the absorption and oxidation of pollutants as well as their resulting compounds. The results regarding the effect of Fe@Fe<sub>2</sub>O<sub>3</sub> amount on the CBZ removal rate indicated that CBZ degradation rate increases with the increase of Fe@Fe<sub>2</sub>O<sub>3</sub> amount (Fig. 7e). This amplified decomposition can be attributed to increased active sites of catalyst surface leading to rapid H<sub>2</sub>O<sub>2</sub> decomposition to hydroxyl radicals and increased level of released iron ions to the solution as well as production of high amounts of hydroxyl radicals via (Fe<sup>2+</sup> + H<sub>2</sub>O<sub>2</sub>) Fenton reaction [42]. Furthermore, this rise in the removal rate can be due to the interaction between nanowires and molecular oxygen for producing ROS such as H<sub>2</sub>O<sub>2</sub>, OH<sup>•</sup> and <sup>•</sup>O<sub>2</sub><sup>-</sup>, according to Eqs. (12)–(15) [30,31].



Typically, these produced oxygen species may oxidize or reduce CBZ in EF process.

Wang et al. [61], investigating the dimethyl phthalate decomposition, reported that by increasing the catalyst concentration, the efficiency of dimethyl phthalate decomposition increased due to the high amount production of radical hydroxyl by Fenton reaction. Jiang et al. [41] concluded, studying the effect of Fe<sub>3</sub>O<sub>4</sub> on the efficiency of color decomposition using the EF process, that increasing catalyst amount, significantly shall increase the color decomposition efficiency rate. He et al. [42] analyzed the EF decomposition using a Fe<sub>3</sub>O<sub>4</sub> catalyst, and their results showed that by catalyst content increase, the efficiency of color decomposition raised due to the radical hydroxyl production growth through the decomposition of H<sub>2</sub>O<sub>2</sub> on the catalyst surface. In a further study by Pourzamani et al. [49], the effect of MWCNTs/Fe<sub>3</sub>O<sub>4</sub> catalyst concentration on the removal of diclofenac by the EF process was investigated. The outcomes showed that by increasing the amount of catalyst, diclofenac decomposition efficiency enhanced due to increasing production of H<sub>2</sub>O<sub>2</sub> and radical hydroxyl. In another research, Shi et al. [30] concluded that in the color decomposition by the Fe@Fe<sub>2</sub>O<sub>3</sub> nanocatalyst via Fenton process, adding Fe@Fe<sub>2</sub>O<sub>3</sub> nanowire to the solution increases the oxidation efficiency of the color. This increase in removal rates can be due to the reaction between the nanowire and molecular oxygen to produce ROS such as <sup>•</sup>O<sub>2</sub><sup>-</sup>, H<sub>2</sub>O<sub>2</sub> and OH<sup>•</sup>. These results are similar with studies performed by Shen et al. [31] on the removal of bromate via Fe@Fe<sub>2</sub>O<sub>3</sub> nanowires. Ding et al. [62] examined electrochemical mineralization of atrazine via Fe@Fe<sub>2</sub>O<sub>3</sub> and demonstrated that Fe@Fe<sub>2</sub>O<sub>3</sub> catalyst had the potential to produce high amounts of H<sub>2</sub>O<sub>2</sub> as well as radical OH by activating molecular oxygen.

In more details, the main role of Fe@Fe<sub>2</sub>O<sub>3</sub> core-shell nanowire is H<sub>2</sub>O<sub>2</sub> generation (activation of two-electron molecular oxygen induced by Fe@Fe<sub>2</sub>O<sub>3</sub> nanowires leads to generate H<sub>2</sub>O<sub>2</sub> via the outward electron transport from iron core to the iron oxide shell surface), and <sup>•</sup>O<sub>2</sub><sup>-</sup> (can be produced by the activation of single-electron molecular oxygen through the surface linkage of ferrous ions to the iron oxide shell) [29,30]. On the one hand, this process is a Fenton-like reaction that requires Fe<sup>2+</sup> ions in which, of course, a portion of them are homogeneously obtained from Fe@Fe<sub>2</sub>O<sub>3</sub> core-shell nanowire [29,30]. In this research, it was demonstrated, by spectrophotometric analysis based on 1,10-phenanthroline, that the amount of released Fe<sup>2+</sup> from the Fe@Fe<sub>2</sub>O<sub>3</sub> core-shell nanowire reaches 0.001 mmol L<sup>-1</sup>. It should be noted that this concentration had been decreased intensively at the beginning of the reaction, which was in agreement with previous studies [32]. Besides, adsorption of produced Fe<sup>2+</sup> from the core into Fe<sub>2</sub>O<sub>3</sub> shell leads to nonsufficient Fe<sup>2+</sup> concentration. Therefore, the produced Fe<sup>2+</sup> by the Fe@Fe<sub>2</sub>O<sub>3</sub> core-shell nanowire is not enough for Fenton reaction. The process promotion, thus, had been evaluated by adding external Fe<sup>2+</sup> [32].

### 3.12. Initial concentrations effect of CBZ

It is known that the pollutant concentration plays an important role in an electrochemical process [53]. Fig. 7f shows that the removal rate of CBZ is slightly reduced from 49.35% to 45.74% by increasing the initial concentration of drug from 7 to 15 mg L<sup>-1</sup>. However the difference of CBZ removal is not very high, this slight decrease in the removal rate of CBZ at high concentrations can be explained by the fact that when all the parameters, including pH, current, FeSO<sub>4</sub>·7H<sub>2</sub>O, Fe@Fe<sub>2</sub>O<sub>3</sub> concentrations and reaction time are constant, a certain amount of radical hydroxyl is produced. This amount of produced OH radical may decompose and remove a certain amount of CBZ. Accordingly, when the initial concentration of the drug increases, the amount of radical OH present in the aqueous solution, is not enough to remove all organic compound molecules [63]. Lei et al. [64] after studying the decomposition of cationic red X-GRL color through the EF process, concluded that, by increasing the initial concentration of the color, the decomposition efficiency decreases due to the constant produced radical hydroxyl and the competition between the intermediates and the main pollutants for produced reactive species. Hou et al. [65] evaluated catechol decomposition by EF process concluding that increased concentration of contaminant reduces decomposition yield. This process is related to physicochemical properties of contaminant and steric effect. Gümüs and Akbal [66] investigated phenol removal by the EF process and reported that by increasing the initial concentration of phenol from 50 to 500 mg L<sup>-1</sup>, the phenol removal efficiency decreased from 98.92% to 68.63%. The researchers also reported that at low concentrations of phenol, the phenol removal efficiency increased due to the high amount of produced radical hydroxyl, while the phenol removal efficiency reduced at high concentrations of contaminants due to increased intermediate productions and its competition with the main contaminant as well as constancy of produced radical hydroxyl amount. Moreover, similar results were

reported by Ouiriemmi et al. [67] for the valinic acid decomposition by the EF process coupled with pyrite, as well as by Wang et al. [61] for the dimethyl phthalate decomposition.

### 3.13. Interaction between variables

The response level plot as a function of two factors at one time and keeping other variables in constant levels help better understanding of the interactions between variables. The curves of response level with the high probability value ( $\text{prob} > F < 0.1$ ) for the CBZ removal are shown in Figs. 8a and b. The elliptical curve displays the proper interaction between two variables and also the circular curve indicates the lack of interactions between the variables [68]. The contour elliptical nature in the graphs indicates the interaction between  $\text{pH} \times \text{FeSO}_4 \cdot 7\text{H}_2\text{O}$  concentration and  $\text{pH} \times \text{reaction time}$ . Results of Fig. 8a on the interaction between  $\text{pH}$  and  $\text{FeSO}_4 \cdot 7\text{H}_2\text{O}$  concentration shows that in different concentrations of  $\text{FeSO}_4 \cdot 7\text{H}_2\text{O}$ , increasing the  $\text{pH}$  reduces the yield of decomposition. This reduced yield can be caused due to formation of ferric oxide and low potential of hydroxyl radicals. Also, this interaction shows that in acidic  $\text{pH}$ , increasing  $\text{FeSO}_4 \cdot 7\text{H}_2\text{O}$  reduces CBZ decomposition yield due to scavenge effect of excess ferrous ions on hydroxyl radicals. Nevertheless, in alkaline  $\text{pH}$ , increased  $\text{FeSO}_4 \cdot 7\text{H}_2\text{O}$  slightly improves CBZ decomposition yield. This increased yield can be attributed to higher participation of ferrous ions in reaction with  $\text{H}_2\text{O}_2$  and formation of more hydroxyl radicals (with low oxidation potential). Finally, these results demonstrate that for treatment of CBZ containing solution, regardless of economic costs, best yield is achieved in  $\text{pH} = 4$  and  $\text{FeSO}_4 \cdot 7\text{H}_2\text{O}$  concentration of  $3 \text{ mg L}^{-1}$ .

Results of interaction between  $\text{pH}$  and reaction time (Fig. 8b) reveals that in different values of  $\text{pH}$ , CBZ decomposition yield increases by increasing of reaction time. This increased yield can be caused due to the production of higher amounts of hydroxyl radicals and higher absorption

of contaminant on  $\text{Fe@Fe}_2\text{O}_3$  nanowires. This interaction indicates that in different reaction times, higher values of  $\text{pH}$  decreases yield of CBZ decomposition. This reduced efficiency may be attributed to formation of ferric oxide and low potential of hydroxyl radicals. The results insist on the fact that highest decomposition yield is achieved in  $\text{pH} = 4$  and reaction time of 50 min. The result of the interaction between  $\text{pH}$  and reaction time (Fig. 8b) shows that at different  $\text{pH}$  values, with increasing response time, the yield of CBZ decomposition increases.

### 3.14. Optimum conditions

Based upon our study carried out by RSM under the fitted linear model of Eq. (7), the maximum (optimized) CBZ decomposition efficiency for its oxidation was achieved (88.55%) at  $\text{pH} = 4$ , current of 0.18 A (current density =  $5.14 \text{ mA cm}^{-2}$ ),  $\text{FeSO}_4 \cdot 7\text{H}_2\text{O}$  concentration of  $3.87 \text{ mg L}^{-1}$ , CBZ concentration of  $7.49 \text{ mg L}^{-1}$ ,  $\text{Fe@Fe}_2\text{O}_3$  dose of  $1,050 \text{ mg L}^{-1}$ , and reaction time of 50 min. These results were confirmed through more experimental runs in the proposed optimized conditions and compared with predicted values.

### 3.15. Stability and reusability test

The  $\text{Fe@Fe}_2\text{O}_3$  core-shell nanowire was examined under optimum conditions ( $\text{pH} = 4$ , current density of  $5.14 \text{ mA cm}^{-2}$ ,  $\text{FeSO}_4 \cdot 7\text{H}_2\text{O}$  concentration of  $3.87 \text{ mg L}^{-1}$ , CBZ concentration of  $7.49 \text{ mg L}^{-1}$ ,  $\text{Fe@Fe}_2\text{O}_3$  dose of  $1,050 \text{ mg L}^{-1}$  and reaction time of 50 min) in terms of stability and reusability through repetitively five experiments, each with the same catalyst. Fig. 9 demonstrates the results, which reveal the fact that the CBZ removal efficiency reduced from 88.55% to 83.76% with an initial increase in the number of cycle runs. Results also suggested that the surface of the used nanowires became rougher, which was likely as a result of generating

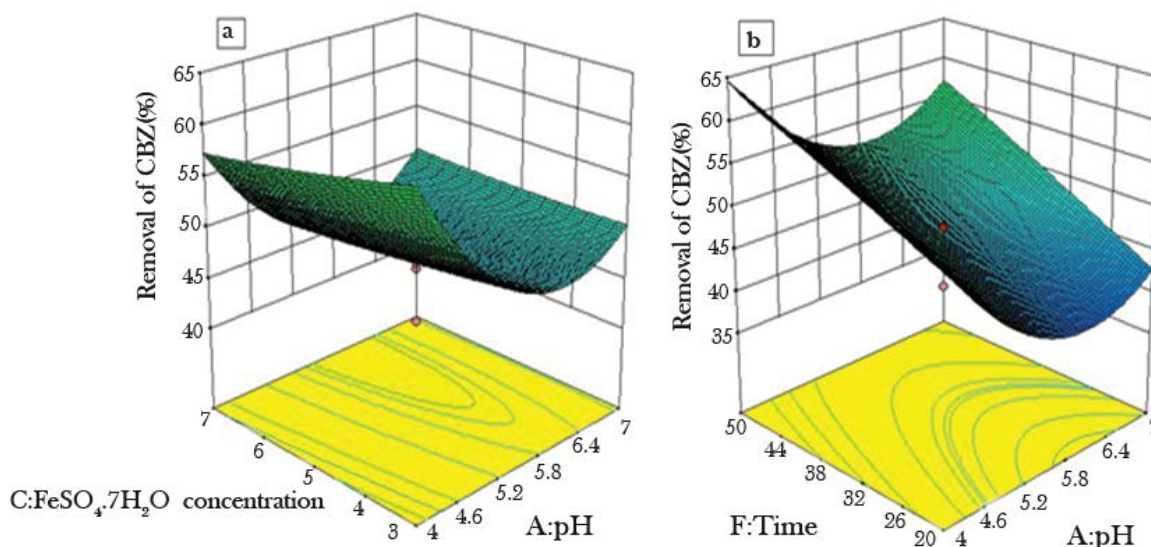


Fig. 8. (a) 3D graph indicating the interaction between  $\text{pH}$  and  $\text{FeSO}_4 \cdot 7\text{H}_2\text{O}$  concentration and (b) interaction between  $\text{pH}$  and reaction time.

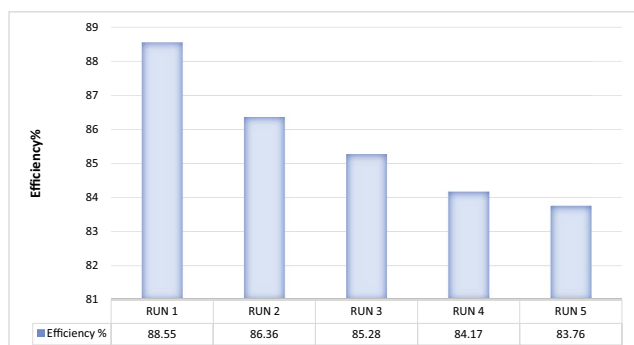


Fig. 9. Stability of Fe@Fe<sub>2</sub>O<sub>3</sub> nanowire in repeated CBZ removal.

new layers of Fe<sub>2</sub>O<sub>3</sub> on the nanowires' surface during the reaction [30].

### 3.16. Degradation pathways

According to a study conducted by Wang et al. [69], several routes for the destruction of CBZ have been proposed, which three routes are more conventional and more important. In this work, using the GC-MS qualitative study, the production of acridine-9-carbaldehyde and also acridine were revealed and thus the CBZ degradation path seems to be done by the first route as shown in Fig. 10.

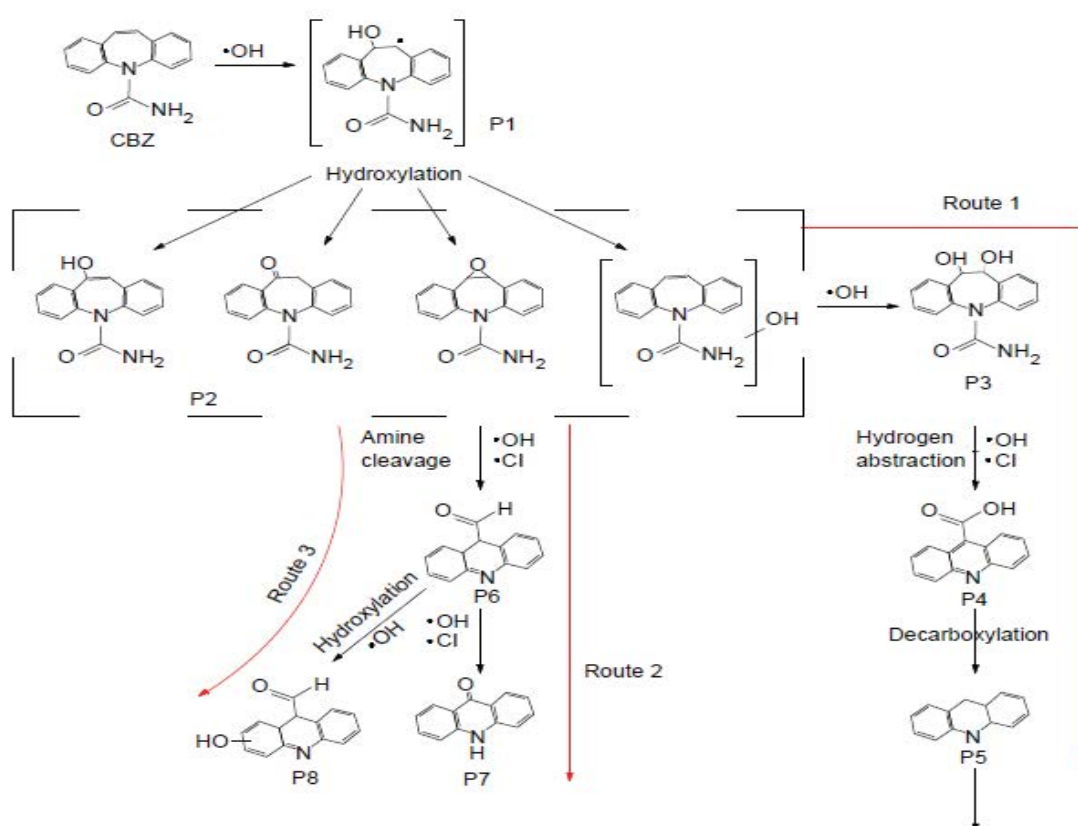


Fig. 10. Intermediates formed during CBZ degradation using EF system. Intermediate named as were P1 = hydroxylation product, P2 = unstable compound, P3 = di-hydroxyl-CBZ, P4 = acridine-9-carbaldehyde, P5 = acridine, P6 = acridine-9-carboxaldehyde, P7 = acridone).

It should be noted that none of the acridine-9-carboxaldehyde, acridone and P8 compounds were detected in this study at different times, and therefore the probability of progressing the reaction path from routes 2 and 3 would be obviated. Also, regarding the acridine production in this reaction, it is necessary to increase the reaction time in order to obtain desirable time to reach the cleavage ring reactions.

### 3.17. TOC removal under optimum conditions

Under optimum conditions (pH = 4, current of 0.18 A (current density = 5.14 mA cm<sup>-2</sup>), FeSO<sub>4</sub>·7H<sub>2</sub>O concentration of 3.87 mg L<sup>-1</sup>, CBZ concentration of 7.49 mg L<sup>-1</sup>, Fe@Fe<sub>2</sub>O<sub>3</sub> dose of 1,050 mg L<sup>-1</sup>, and reaction time of 50 min), the obtained TOC removal efficiencies were 65%. In other words, the strategy for optimizing drug decomposition and achieving maximum decomposition efficiency by RSM for CBZ oxidation through the EF process in the presence of Fe@Fe<sub>2</sub>O<sub>3</sub> nanowires was successful.

## 4. Conclusion

In this study, EF treatment of CBZ via Ti/PbO<sub>2</sub> anode and catalyst of Fe@Fe<sub>2</sub>O<sub>3</sub> nanowire was evaluated. Ti/PbO<sub>2</sub> electrode and Fe@Fe<sub>2</sub>O<sub>3</sub> were prepared by electro deposition process and co-precipitation, respectively. XRD and SEM-EDS analysis showed that the electrodes were properly

synthesized in accordance with former studies. The best condition for CBZ removal was pH = 4, current = 0.18 A (current density = 5.14 mA cm<sup>-2</sup>), FeSO<sub>4</sub>·7H<sub>2</sub>O concentration = 3.87 mg L<sup>-1</sup>, CBZ concentration = 7.49 mg L<sup>-1</sup>, Fe@Fe<sub>2</sub>O<sub>3</sub> dose = 1,050 mg L<sup>-1</sup> and reaction time = 50 min. Variance analysis disclosed that a second-tier empirical regression model could adequately interpret laboratory data with determination coefficients (*R*<sup>2</sup>) of 0.918 and *F* = 87.84. The results on the interactions revealed the interactions between pH with FeSO<sub>4</sub>·7H<sub>2</sub>O concentration and pH with reaction time. In a nutshell, the results suggested that EF process catalyzed by Fe@Fe<sub>2</sub>O<sub>3</sub> nanowire can be used for the removal of pharmaceutical compounds such as CBZ from aqueous solutions. The main advantage of the current work is using multivariate approach for optimization, which led to deeper view on the effective parameters that may be applied for further mechanistic investigations in the removal of CBZ in the integrated advanced oxidizing process.

### Acknowledgment

The authors are grateful for the financial support from the Isfahan University of Medical Sciences, Isfahan, Iran; Research Project # 396006.

### References

- Y. Rao, H. Yang, D. Xue, Y. Guo, F. Qi, J. Ma, Sonolytic and sonophotolytic degradation of carbamazepine: kinetic and mechanisms, *Ultrason. Sonochem.*, 32 (2016) 371–379.
- R.S. Rana, P. Singh, V. Kandari, R. Singh, R. Dobhal, S. Gupta, A review on characterization and bioremediation of pharmaceutical industries' wastewater: an Indian perspective, *Appl. Water Sci.*, 7 (2017) 1–12.
- V.M. Monsalvo, J. Lopez, M. Munoz, Z.M. de Pedro, J.A. Casas, A.F. Mohedano, J.J. Rodriguez, Application of Fenton-like oxidation as pre-treatment for carbamazepine biodegradation, *Chem. Eng. J.*, 264 (2015) 856–862.
- S. Wang, N. Zhou, Removal of carbamazepine from aqueous solution using sono-activated persulfate process, *Ultrason. Sonochem.*, 29 (2016) 156–162.
- Y. Zhang, S.-U. Geißen, C. Gal, Carbamazepine and diclofenac: removal in wastewater treatment plants and occurrence in water bodies, *Chemosphere*, 73 (2008) 1151–1161.
- J.R. Domínguez, T. González, P. Palo, E.M. Cuerda-Correa, Fenton + Fenton-like integrated process for carbamazepine degradation: optimizing the system, *Ind. Eng. Chem. Res.*, 51 (2012) 2531–2538.
- P. Braeutigam, M. Franke, R.J. Schneider, A. Lehmann, A. Stolle, B. Ondruschka, Degradation of carbamazepine in environmentally relevant concentrations in water by Hydrodynamic-Acoustic-Cavitation (HAC), *Water Res.*, 46 (2012) 2469–2477.
- P. Oleszczuk, B. Pan, B. Xing, Adsorption and desorption of oxytetracycline and carbamazepine by multiwalled carbon nanotubes, *Environ. Sci. Technol.*, 43 (2009) 9167–9173.
- I. Vergili, Application of nanofiltration for the removal of carbamazepine, diclofenac and ibuprofen from drinking water sources, *J. Environ. Manage.*, 127 (2013) 177–187.
- L. Hu, H.M. Martin, O. Arce-Bulted, M.N. Sugihara, K.A. Keating, T.J. Strathmann, Oxidation of carbamazepine by Mn(VII) and Fe(VI): reaction kinetics and mechanism, *Environ. Sci. Technol.*, 43 (2009) 509–515.
- A. Carabin, P. Drogui, D. Robert, Photocatalytic oxidation of carbamazepine: application of an experimental design methodology, *Water Air Soil Pollut.*, 227 (2016) 122.
- A. Özcan, Y. Şahin, A.S. Kopalal, M.A. Oturan, A comparative study on the efficiency of electro-Fenton process in the removal of prophan from water, *Appl. Catal., B*, 89 (2009) 620–626.
- P.V. Nidheesh, Graphene-based materials supported advanced oxidation processes for water and wastewater treatment: a review, *Environ. Sci. Pollut. Res.*, 24 (2017) 27047–27069.
- B. Bethi, S.H. Sonawane, B.A. Bhanvase, S.P. Gumfekar, Nanomaterials-based advanced oxidation processes for wastewater treatment: a review, *Chem. Eng. Process. Process Intensif.*, 109 (2016) 178–189.
- P.V. Nidheesh, R. Gandhimathi, Trends in electro-Fenton process for water and wastewater treatment: an overview, *Desalination*, 299 (2012) 1–15.
- W.-P. Ting, M.-C. Lu, Y.-H. Huang, Kinetics of 2,6-dimethylaniline degradation by electro-Fenton process, *J. Hazard. Mater.*, 161 (2009) 1484–1490.
- E. Bocos, O. Iglesias, M. Pazos, M. Ángeles Sanromán, Nickel foam a suitable alternative to increase the generation of Fenton's reagents, *Process Saf. Environ. Prot.*, 101 (2016) 34–44.
- J. Anotai, S. Singhadech, C.-C. Su, M.-C. Lu, Comparison of o-toluidine degradation by Fenton, electro-Fenton and photo-electro-Fenton processes, *J. Hazard. Mater.*, 196 (2011) 395–401.
- P. V. Nidheesh, M. Zhou, M.A. Oturan, An overview on the removal of synthetic dyes from water by electrochemical advanced oxidation processes, *Chemosphere*, 197 (2018) 210–227.
- S. Vasudevan, M.A. Oturan, Electrochemistry: as cause and cure in water pollution-an overview, *Environ. Chem. Lett.*, 12 (2014) 97–108.
- S. Karthikeyan, A. Titus, A. Gnanamani, A.B. Mandal, G. Sekaran, Treatment of textile wastewater by homogeneous and heterogeneous Fenton oxidation processes, *Desalination*, 281 (2011) 438–445.
- M. Muruganandham, R.P.S. Suri, M. Sillanpää, J.J. Wu, B. Ahmmad, S. Balachandran, M. Swaminathan, Recent developments in heterogeneous catalyzed environmental remediation processes, *J. Nanosci. Nanotechnol.*, 14 (2014) 1898–1910.
- P. V. Nidheesh, Heterogeneous Fenton catalysts for the abatement of organic pollutants from aqueous solution: a review, *RSC Adv.*, 5 (2015) 40552–40577.
- G. Bonyadinejad, M. Sarafraz, M. Khosravi, A. Ebrahimi, S.M. Taghavi-Shahri, R. Nateghi, S. Rastaghi, Electrochemical degradation of the Acid Orange 10 dye on a Ti/PbO<sub>2</sub> anode assessed by response surface methodology, *Korean J. Chem. Eng.*, 33 (2016) 189–196.
- A.M. Polcaro, S. Palmas, F. Renoldi, M. Mascia, On the performance of Ti/SnO<sub>2</sub> and Ti/PbO<sub>2</sub> anodes in electrochemical degradation of 2-chlorophenol for wastewater treatment, *J. Appl. Electrochem.*, 29 (1999) 147–151.
- C. Barrera-Díaz, P. Cañizares, F.J. Fernández, R. Natividad, M.A. Rodrigo, Electrochemical advanced oxidation processes: an overview of the current applications to actual industrial effluents, *J. Mex. Chem. Soc.*, 58 (2014) 256–275.
- B. Hou, H. Han, H. Zhuang, P. Xu, S. Jia, K. Li, A novel integration of three-dimensional electro-Fenton and biological activated carbon and its application in the advanced treatment of biologically pretreated Lurgi coal gasification wastewater, *Bioresour. Technol.*, 196 (2015) 721–725.
- B. Hou, B. Ren, R. Deng, G. Zhu, Z. Wang, Z. Li, Three-dimensional electro-Fenton oxidation of N-heterocyclic compounds with a novel catalytic particle electrode: high activity, wide pH range and catalytic mechanism, *RSC Adv.*, 7 (2017) 15455–15462.
- Z. Ai, Z. Gao, L. Zhang, W. He, J.J. Yin, Core-shell structure dependent reactivity of Fe@Fe<sub>2</sub>O<sub>3</sub> nanowires on aerobic degradation of 4-chlorophenol, *Environ. Sci. Technol.*, 47 (2013) 5344–5352.
- J. Shi, Z. Ai, L. Zhang, Fe@Fe<sub>2</sub>O<sub>3</sub> core-shell nanowires enhanced Fenton oxidation by accelerating the Fe(III)/Fe(II) cycles, *Water Res.*, 59 (2014) 145–153.
- W. Shen, F. Lin, X. Jiang, H. Li, Z. Ai, L. Zhang, Efficient removal of bromate with core-shell Fe@Fe<sub>2</sub>O<sub>3</sub> nanowires, *Chem. Eng. J.*, 308 (2017) 880–888.
- W. Liu, Z. Ai, M. Cao, L. Zhang, Ferrous ions promoted aerobic simazine degradation with Fe@Fe<sub>2</sub>O<sub>3</sub> core-shell nanowires, *Appl. Catal., B*, 150–151 (2014) 1–11.



- [33] L. Zhu, Z. Ai, W. Ho, L. Zhang, Core-shell Fe-Fe<sub>3</sub>O<sub>4</sub> nanostructures as effective persulfate activator for degradation of methyl orange, *Sep. Purif. Technol.*, 108 (2013) 159–165.
- [34] M. Panizza, C.A. Martinez-Huitle, Role of electrode materials for the anodic oxidation of a real landfill leachate – comparison between Ti–Ru–Sn ternary oxide, PbO<sub>2</sub> and boron-doped diamond anode, *Chemosphere*, 90 (2013) 1455–1460.
- [35] Z. Ai, Y. Cheng, L. Zhang, J. Qiu, Efficient removal of Cr(VI) from aqueous solution with Fe@Fe<sub>3</sub>O<sub>4</sub> core-shell nanowires, *Environ. Sci. Technol.*, 42 (2008) 6955–6960.
- [36] Z. Ai, L. Lu, J. Li, L. Zhang, J. Qiu, M. Wu, Fe@Fe<sub>3</sub>O<sub>4</sub> Core-shell nanowires as the iron reagent. 2. An efficient and reusable sono-fenton system working at neutral pH, *J. Phys. Chem. C*, 111 (2007) 7430–7436.
- [37] Z. Ai, L. Lu, J. Li, L. Zhang, J. Qiu, M. Wu, Fe@Fe<sub>3</sub>O<sub>4</sub> Core-shell nanowires as iron reagent. 1. Efficient degradation of rhodamine B by a novel sono-Fenton process, *J. Phys. Chem. C*, 111 (2007) 4087–4093.
- [38] G. Bonyadinejad, M. Khosravi, A. Ebrahimi, R. Nateghi, S.M. Taghavi-Shahri, H. Mohammadi, Sono-electrochemical mineralization of perfluorooctanoic acid using Ti/PbO<sub>2</sub> anode assessed by response surface methodology, *J. Environ. Health Sci. Eng.*, 13 (2015) 77.
- [39] S. Yousefinejad, F. Honarasa, H. Montaseri, Linear solvent structure-polymer solubility and solvation energy relationships to study conductive polymer/carbon nanotube composite solutions, *RSC Adv.*, 5 (2015) 42266–42275.
- [40] E. Alfaya, O. Iglesias, M. Pazos, M.A. Sanromán, Environmental application of an industrial waste as catalyst for the electro-Fenton-like treatment of organic pollutants, *RSC Adv.*, 5 (2015) 14416–14424.
- [41] H. Jiang, Y. Sun, J. Feng, J. Wang, Heterogeneous electro-Fenton oxidation of azo dye methyl orange catalyzed by magnetic Fe<sub>3</sub>O<sub>4</sub> nanoparticles, *Water Sci. Technol.*, 74 (2016) 1116–1126.
- [42] Z. He, C. Gao, M. Qian, Y. Shi, J. Chen, S. Song, Electro-Fenton process catalyzed by Fe<sub>3</sub>O<sub>4</sub> magnetic nanoparticles for degradation of C.I. Reactive Blue 19 in aqueous solution: operating conditions, influence, and mechanism, *Ind. Eng. Chem. Res.*, 53 (2014) 3435–3447.
- [43] Z. Ai, T. Mei, J. Liu, J. Li, F. Jia, L. Zhang, J. Qiu, Fe@Fe<sub>3</sub>O<sub>4</sub> Core-shell nanowires as an iron reagent. 3. Their combination with CNTs as an effective oxygen-fed gas diffusion electrode in a neutral electro-Fenton system, *J. Phys. Chem. C*, 111 (2007) 14799–14803.
- [44] H. Zhao, Y. Wang, Y. Wang, T. Cao, G. Zhao, Electro-Fenton oxidation of pesticides with a novel Fe<sub>3</sub>O<sub>4</sub>@Fe<sub>2</sub>O<sub>3</sub>/activated carbon aerogel cathode: High activity, wide pH range and catalytic mechanism, *Appl. Catal., B*, 125 (2012) 120–127.
- [45] M. Panizza, G. Cerisola, Electro-Fenton degradation of synthetic dyes, *Water Res.*, 43 (2009) 339–344.
- [46] P.V. Nidheesh, R. Gandhimathi, S. Velmathi, N.S. Sanjini, Magnetite as a heterogeneous electro Fenton catalyst for the removal of Rhodamine B from aqueous solution, *RSC Adv.*, 4 (2014) 5698–5708.
- [47] F. Yu, M. Zhou, X. Yu, Cost-effective electro-Fenton using modified graphite felt that dramatically enhanced on H<sub>2</sub>O<sub>2</sub> electro-generation without external aeration, *Electrochim. Acta*, 163 (2015) 182–189.
- [48] M.S. Yahya, N. Beqqal, A. Guessous, M.R. Arhoutane, K. El Kacemi, Degradation and mineralization of moxifloxacin antibiotic in aqueous medium by electro-Fenton process: kinetic assessment and oxidation products, *Cogent Chem.*, 144 (2017) 1–11.
- [49] H. Pourzamani, Y. Hajizadeh, N. Mengelizadeh, Application of three-dimensional electro-fenton process using MWCNTs-Fe<sub>3</sub>O<sub>4</sub> nanocomposite for removal of diclofenac, *Process Saf. Environ. Prot.*, 119 (2018) 271–284.
- [50] T. Sruthi, R. Gandhimathi, S.T. Ramesh, P.V. Nidheesh, Stabilized landfill leachate treatment using heterogeneous Fenton and electro-Fenton processes, *Chemosphere*, 210 (2018) 38–43.
- [51] C. García-Gómez, P. Drogui, F. Zavisca, B. Seyhi, P. Gortáres-Moroyoqui, G. Buelna, C. Neira-sáenz, M. Estrada-Alvarado, R.G. Ulloa-Mercado, Experimental design methodology applied to electrochemical oxidation of carbamazepine using Ti/PbO<sub>2</sub> and Ti/BDD electrodes, *J. Electroanal. Chem.*, 732 (2014) 1–10.
- [52] C. Jiang, J. Zhang, Progress and prospect in electro-Fenton process for wastewater treatment, *J. Zhejiang Univ. Sci. A*, 8 (2007) 1118–1125.
- [53] Ö. Gökkuş, Y.Ş. Yıldız, Application of electro-Fenton process for medical waste sterilization plant wastewater, *Desal. Wat. Treat.*, 57 (2016) 24934–24945.
- [54] E. Bocos, M. Pazos, M.Á. Sanromán, Electro-Fenton treatment of imidazolium-based ionic liquids: kinetics and degradation pathways, *RSC Adv.*, 6 (2016) 1958–1965.
- [55] C. Zhang, M. Zhou, G. Ren, X. Yu, L. Ma, J. Yang, F. Yu, Heterogeneous electro-Fenton using modified iron-carbon as catalyst for 2,4-dichlorophenol degradation: influence factors, mechanism and degradation pathway, *Water Res.*, 70 (2015) 414–424.
- [56] O. Iglesias, J. Gómez, M. Pazos, M.Á. Sanromán, Electro-Fenton oxidation of imidacloprid by Fe alginate gel beads, *Appl. Catal., B*, 144 (2014) 416–424.
- [57] C.-T. Wang, W.-L. Chou, M.-H. Chung, Y.-M. Kuo, COD removal from real dyeing wastewater by electro-Fenton technology using an activated carbon fiber cathode, *Desalination*, 253 (2010) 129–134.
- [58] M. Zhou, Q. Yu, L. Lei, G. Barton, Electro-Fenton method for the removal of methyl red in an efficient electrochemical system, *Sep. Purif. Technol.*, 57 (2007) 380–387.
- [59] F. Iranpour, H. Pourzamani, N. Mengelizadeh, P. Bahrami, H. Mohammadi, Application of response surface methodology for optimization of reactive black 5 removal by three dimensional electro-Fenton process, *J. Environ. Chem. Eng.*, 6 (2018) 3418–3435.
- [60] H. Mohammadi, B. Bina, A. Ebrahimi, A novel three-dimensional electro-Fenton system and its application for degradation of anti-inflammatory pharmaceuticals: modeling and degradation pathways, *Process Saf. Environ. Prot.*, 117 (2018) 200–213.
- [61] Y. Wang, Y. Liu, T. Liu, S. Song, X. Gui, H. Liu, P. Tsiakaras, Dimethyl phthalate degradation at novel and efficient electro-Fenton cathode, *Appl. Catal., B*, 156–157 (2014) 1–7.
- [62] X. Ding, S. Wang, W. Shen, Y. Mu, L. Wang, H. Chen, L. Zhang, Fe@Fe<sub>3</sub>O<sub>4</sub> promoted electrochemical mineralization of atrazine via a triazinon ring opening mechanism, *Water Res.*, 112 (2017) 9–18.
- [63] M. Malakootian, A. Moridi, Efficiency of electro-Fenton process in removing Acid Red 18 dye from aqueous solutions, *Process Saf. Environ. Prot.*, 111 (2017) 138–147.
- [64] H. Lei, H. Li, Z. Li, Z. Li, K. Chen, X. Zhang, H. Wang, Electro-Fenton degradation of cationic red X-GRL using an activated carbon fiber cathode, *Process Saf. Environ. Prot.*, 88 (2010) 431–438.
- [65] B. Hou, H. Han, S. Jia, H. Zhuang, P. Xu, D. Wang, Heterogeneous electro-Fenton oxidation of catechol catalyzed by nano-Fe<sub>3</sub>O<sub>4</sub>: kinetics with the Fermi's equation, *J. Taiwan Inst. Chem. Eng.*, 56 (2015) 138–147.
- [66] D. Gümüş, F. Akbal, Comparison of Fenton and electro-Fenton processes for oxidation of phenol, *Process Saf. Environ. Prot.*, 103 (2016) 252–258.
- [67] I. Ouiriemmi, A. Karrab, N. Oturan, M. Pazos, E. Rozales, A. Gadri, M.Á. Sanromán, S. Ammar, M.A. Oturan, Heterogeneous electro-Fenton using natural pyrite as solid catalyst for oxidative degradation of vanillic acid, *J. Electroanal. Chem.*, 797 (2017) 69–77.
- [68] S. Sathian, G. Radha, V. Shanmugapriya, M. Rajasimman, C. Karthikeyan, Optimization and kinetic studies on treatment of textile dye wastewater using *Pleurotus floridanus*, *Appl. Water Sci.*, 3 (2013) 41–48.
- [69] W. Wang, Q. Wu, N. Huang, T. Wang, H. Hu, Synergistic effect between UV and chlorine (UV/chlorine) on the degradation of carbamazepine: Influence factors and radical species, *Water Res.*, 98 (2016) 190–198.

## Supplementary Information

Table S1  
 Experimental design with Fe@Fe<sub>2</sub>O<sub>3</sub> nanowire electro Fenton process

Run	pH	Current, A	FeSO <sub>4</sub> ·7H <sub>2</sub> O (mg L <sup>-1</sup> )	CBZ (mg L <sup>-1</sup> )	Fe@Fe <sub>2</sub> O <sub>3</sub> (mg L <sup>-1</sup> )	Contact time (min)	Removing yield (%)
1	4	0.2	7	7	1,050	50	79.456
2	4	0.1	7	15	350	20	44.591
3	4	0.2	3	7	350	20	58.77
4	4	0.1	3	15	350	50	52.76
5	7	0.2	7	7	350	20	39.691
6	4	0.2	3	15	350	20	46.54
7	7	0.2	7	7	1,050	20	54.934
8	4	0.1	7	15	1,050	20	54.729
9	7	0.2	7	15	350	20	36.81
10	4	0.2	7	7	350	50	56.76
11	5.5	0.15	5	11	700	35	46.694
12	7	0.2	7	7	350	50	54.14
13	7	0.1	3	7	1,050	50	61.21
14	7	0.1	7	7	1,050	20	50.77
15	5.5	0.15	5	11	700	5	32.39
16	4	0.2	3	15	350	50	56.77
17	7	0.2	3	15	1,050	20	53.578
18	4	0.1	3	7	350	20	42.132
19	5.5	0.15	5	11	700	35	46.04
20	7	0.1	3	7	1,050	20	46.55
21	7	0.2	3	7	350	50	54.293
22	7	0.1	3	7	350	50	51.759
23	4	0.1	7	7	1,050	20	62.44
24	2.5	0.15	5	11	700	35	98.95
25	7	0.1	7	15	350	50	47.85
26	4	0.1	7	7	350	50	53.14
27	4	0.1	7	7	350	20	37.765
28	7	0.2	3	7	350	20	43.11
29	4	0.2	3	15	1,050	50	76.429
30	5.5	0.15	5	11	700	35	40.68
31	7	0.1	3	7	350	20	36.67
32	4	0.2	7	15	350	20	48.65
33	5.5	0.15	5	11	700	65	62.12
34	4	0.2	7	15	1,050	20	61.276
35	7	0.1	3	15	350	20	33.761
36	4	0.2	3	7	1,050	20	72.22
37	7	0.1	7	7	350	50	51.433
38	4	0.2	3	15	1,050	20	64.32
39	7	0.1	7	15	350	20	31.398
40	4	0.2	7	15	350	50	47.31
41	7	0.1	3	15	1,050	20	51.43
42	4	0.2	3	7	1,050	50	84.32
43	4	0.2	3	7	350	50	66.87
44	7	0.2	3	15	1,050	50	67.541
45	5.5	0.15	5	11	1,400	35	74.76
46	5.5	0.15	9	11	700	35	47.87

(Table S1 Continued)

Table S1 Continued

Run	pH	Current density A cm <sup>-2</sup>	FeSO <sub>4</sub> ·7H <sub>2</sub> O (mg L <sup>-1</sup> )	CBZ (ppm)	Fe@Fe <sub>2</sub> O <sub>3</sub> (mg L <sup>-1</sup> )	Contact time (min)	Removing yield (%)
47	7	0.2	7	15	1,050	50	70.439
48	7	0.2	3	15	350	50	51.89
49	4	0.1	7	15	350	50	56.65
50	4	0.1	3	7	1,050	50	78.89
51	7	0.2	3	15	350	20	36.65
52	7	0.2	3	7	1,050	50	70.497
53	5.5	0.15	5	11	0	35	30.42
54	8.5	0.15	5	11	700	35	61.24
55	7	0.2	7	7	1,050	50	66.743
56	4	0.1	3	15	1,050	50	71.33
57	4	0.1	7	7	1,050	50	76.55
58	4	0.2	7	15	1,050	50	72.128
59	5.5	0.15	5	19	700	35	42.43
60	4	0.2	7	7	350	20	42.365
61	4	0.1	3	7	1,050	20	68.32
62	7	0.1	3	15	1,050	50	65.66
63	7	0.1	7	7	350	20	34.65
64	7	0.1	7	15	1,050	20	48.81
65	4	0.1	7	15	1,050	50	63.43
66	7	0.2	3	7	1,050	20	57.34
67	7	0.2	7	15	350	50	52.55
68	7	0.1	7	7	1,050	50	69.92
69	5.5	0.15	5	11	700	35	47.7
70	5.5	0.15	1	11	700	35	50.79
71	4	0.1	3	7	350	50	51.54
72	7	0.1	7	15	1,050	50	60.43
73	4	0.2	7	7	1,050	20	64.543
74	5.5	0.25	5	11	700	35	55.53
75	7	0.1	3	15	350	50	49.66
76	5.5	0.15	5	3	700	35	59.42
77	4	0.1	3	15	350	20	44.65
78	7	0.2	7	15	1,050	20	62.89
79	5.5	0.15	5	11	700	35	47.87
80	5.5	0.05	5	11	700	35	36.88
81	4	0.1	3	15	1,050	20	60.76